Japanese Journal of Applied Physics
Vol. 47, No. 6, 2008, pp. 0000–0000

Microwave Absorption of Catalyst in a Thermal Decomposition Reaction by Recursive Transfer Method

Hatsuhiro KATO and Yoshinori KANNO

Interdisciplinary Graduate School of Medicine and Engineering, University of Yamanashi, 4-3-11 Takeda, Kofu 400-8511, Japan

(Received November 23, 2007; accepted February 21, 2008; published online xxxx yy, zzzz)

The microwave heating of the catalyst in a decomposition reactor is analyzed using a microwave theory of the recursive transfer method. The feature of the catalyst film is expressed using an effective dielectric constant and an effective conductance. It is pointed out that the heating of the catalyst is determined by the effective skin depth and diameter of the container tube. [DOI: 10.1143/JJAP.47.dummy]

KEYWORDS: thermal decomposition, volatile organic compounds, microwave, catalyst

1. Introduction

The use of microwave irradiation in catalytic reactions, including the decomposition of a volatile organic compound, has given some remarkable results.[1–3] The commonly used materials for microwave thermal decomposition processes are alumina and quartz sand. Because the catalyst should exclusively absorb the microwave power, the carrier materials should be transmitting, which is characterized by a small loss-tangent. The latter is 0.057 for alumina, And 0.070 for quartz sand.[4] Both alumina and quartz are weak absorbers if the purity is sufficiently high.

To assist the microwave absorption, a metallic film coating the catalyst grain is effective, and its film thickness is important. If the film thickness is too thick, most of the microwave will be reflected on the film surface. The factors associated with the dissociation rate of volatile organic compounds are the evaluation of the microwave absorption and the variation of temperature on the film surface. Many researchers have studied the effect of microwave heating on catalytic reactions.[5,6] However, the effect of the metal film on the temperature was not taken into consideration. We have analyzed the power absorption against the film thickness with a model for a catalyst grain.[7] Here, we have improved this model and developed a method to deal with the assembly of the grain using the effective dielectric constant and conductivity. In this paper, the absorption of microwave power is considered as a scattering problem within the framework of the recursive transfer method.[8] The calculated absorption power is compared with the measured temperature of the catalyst obtained using a novel sensor applicable under a microwave irradiation field. Here, the temperature is assumed to be proportional to the microwave absorption.

2. Experimental Configuration and Results

$Ni(NO_3)\cdot 6H_2O$ was used as a precursor for the Ni catalysts. Ni catalyst of various weights (2, 5, 8, 10, 15, 20, and 30%) were mixed with the carrier particles (200 μm quartz sand; Nippon Steel Trading) and excess distilled water. The thickness of the film was calculated and shown in Table I. The catalysts were dried at 313–323 K using an infrared lamp for 3 h. After drying, they were dried again overnight at 393 K in air to evaporate the water within the catalysts completely. After the long drying period, the catalysts were calcined in two different ways in order to prepare the different crystallinity materials. One calcination method involved the catalysts being calcined in air at 673 K for 1 h in order to release NO and NO_2 completely. Then, the catalysts were reduced in pure hydrogen at 773 K for 5 h. The other method involves the catalysts being calcined in pure hydrogen at 573 K for 6 h. Before the reaction, the microwave was irradiated on the catalysts for 10 min at 200 W to reduce the metal oxides using hydrogen (activation treatment). The experimental apparatus is shown in Fig. 1. The catalysts were heated by microwave irradiation in the fixed-bed into the quartz glass reactor. The catalysts were placed on the position where the microwave power was mostly focused. The end of the quartz tube was equipped with a new thermosensor developed in the Kanno lab. This sensor can be used to measure the temperature under microwave irradiation. The edge of the thermosensor was installed into the catalyst and fixed using Kao wool (Al_2O_3–SiO_2 wool). The catalyst was also held using Kao wool in

Table I. Estimation of catalyst film thickness on carrier.

Ni catalyst (wt %)	2	5	8	10	15	20	30
Film thickness (μm)	0.2	0.52	0.86	1.09	1.72	2.42	4.09

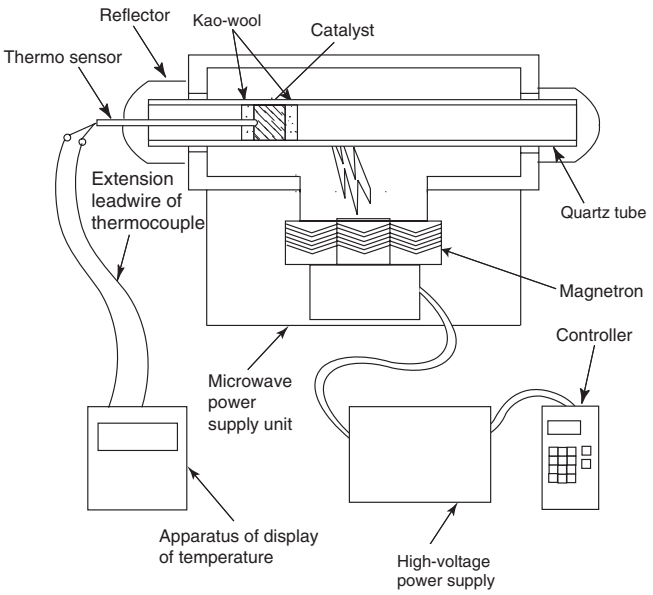

Fig. 1. Thermal analyser for microwave heating system.

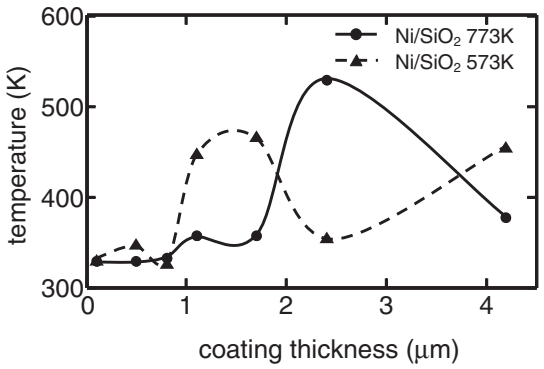

Fig. 2. Relationship between coating thickness of Ni film and film temperature (data from ref. 7). Lines are visual guides.

the quartz tube. The total weight of the catalyst and carrier was 4.0 g. Microwave power was set at 120 W. To ensure that the thermal environment of catalysis is in the steady state, the temperature was measured after the catalysis was exposed to the microwave for about five minutes. The results were obtained as shown in Fig. 2. It shows that the Ni catalysts coated on SiO_2 carriers of 200 μm diameter were not enough to absorb sufficient microwave power. As for Ni/SiO_2 catalysts calcined at 773 K, the highest temperature of the Ni film was around 2.5 μm. On the other hand, the data for the film calcined at 573 K reduced its maximum temperature compared with the data for the film calcinated at 773 K. Our model explains the variation of the temperature related to the skin depth and the diameter of the quartz tube.

3. Grain Model and Absorption Formulation

3.1 *Model of catalyst grain*

Figure 3 shows a model of the catalyst grain, where the catalyst is assumed to be a sphere with necks linking the adjacent grains (a). The grain is composed of a quartz core with a radius R_s and nickel-coated film with a thickness l. The assembly of the catalyst is characterized phenomenologically by the dielectric constant and the conductivity under microwave irradiation (b), where the unit structure is cubic with the dimension $d = 2(R_s + l)$. The gathered catalyst grains are assumed to be a compound of metal and quartz (c). The conductance of the catalyst grains depends on the network of resistances. These resistances are due to the coated metal film, r_{coat}, and the grain neck, r_{neck}, owing to insufficient contact between adjacent grains. The former resistance is expressed as $r_{coat} = \kappa\rho/l$ with ρ the specific resistance of the coating film and κ a proportionality constant. Here, a parameter defined by $\rho_{cr} = \kappa\rho$ is introduced as a fitting parameter. Then, the grains in the close-packed structure have the resistance of $r_{eff} = (r_{neck} + r_{coat})/2$ and the conductance of the grains in network is effectively given as $\sigma_{eff} = (\sqrt{2}dr_{eff})^{-1}$, which can be expressed as

$$\sigma_{eff} = \frac{1}{\sqrt{2}(R_s + l)(r_{neck} + \rho_{cr}/l)}. \quad (1)$$

A single element of metal (quartz) sphere with volume v_m (v_s) under an external field has the polarizability α_m (α_s) of

$$\alpha_m = 3\epsilon_0 v_m, \quad \alpha_s = 3\epsilon_0 v_s \frac{\epsilon_s - \epsilon_0}{\epsilon_s + 2\epsilon_0}, \quad (2)$$

where ϵ_0 and ϵ_s are the dielectric constants of the vacuum and quartz, respectively. According to the Clausius–Mossotti relation,[9] the effective dielectric constant ϵ_{eff} of the compound satisfies the relation

$$\frac{\epsilon_{eff} - \epsilon_0}{\epsilon_{eff} + 2\epsilon_0} = \frac{1}{3\epsilon_0}(n_m\alpha_m + n_s\alpha_s), \quad (3)$$

where n_m and n_s are numbers of metal and quartz elements per unit volume, respectively. Therefore, the effective dielectric constant is obtained using

$$\epsilon_{eff} = \epsilon_0 \frac{1 + 2f}{1 - f}, \quad (4)$$

where f is a factor defined as

$$f = n_m v_m + n_s v_s \frac{\epsilon_s - \epsilon_0}{\epsilon_s + 2\epsilon_0}, \quad (5)$$

with the space occupation of f metal, $n_m v_m$, and quartz, $n_s v_s$. If the catalyst grains are gathered in the close-packed structure as shown in Fig. 3(b), the space-filling factors are given by

$$n_m v_m = \frac{\pi}{3\sqrt{2}}\left[1 - \left(\frac{R_s}{R_s + l}\right)^3\right], \quad n_s v_s = \frac{\pi}{3\sqrt{2}}\left(\frac{R_s}{R_s + l}\right)^3. \quad (6)$$

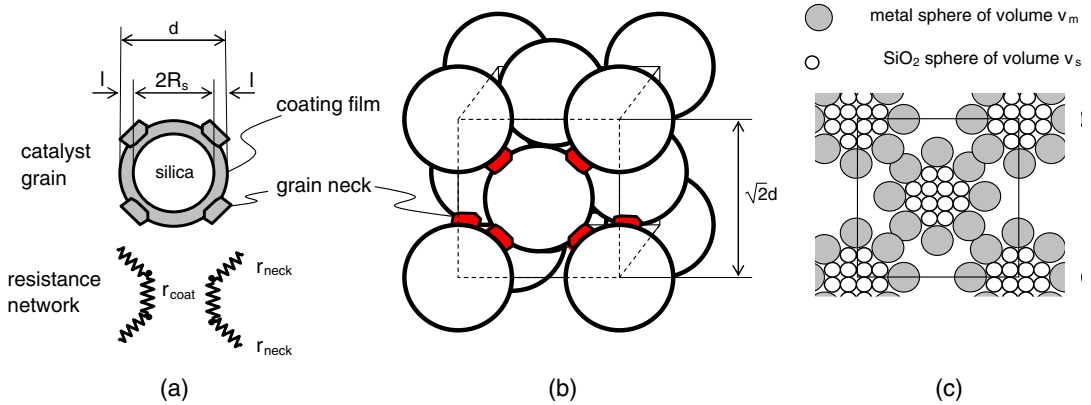

Fig. 3. (Color online) Model of catalyst grains. (a) Resistances of a single grain, (b) closed-packed structure of gathered grains, and (c) elemental spheres of metal and quartz to compose the grains.

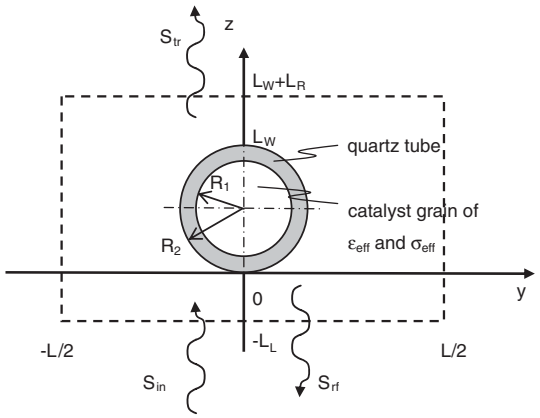

Fig. 4. Model configuration of quartz tube filled with catalyst grains.

3.2 Microwave penetration and reflection

Figure 4 shows a model of the irradiated quartz tube, where the microwave propagates along the z-axis. The tube has an inner radius R_1 and an external radius R_2. The tube is filled with catalyst grains of dielectric constant ϵ_{eff} and conductance σ_{eff}. If the electric field $\mathbf{E}$ is polarized along the x-axis and expressed as $E = (\Phi(z, y)e^{-i\omega t}, 0, 0)$, the field component $\Phi(z, y)$ satisfies

$$\left(\frac{\partial^2}{\partial z^2} + \frac{\partial^2}{\partial y^2}\right)\Phi + V_{\text{sc}}\Phi + \omega^2\epsilon_0\mu_0\Phi = 0. \tag{7}$$

Here, μ_0 is the permeability of vacuum, ω is the angular frequency, and $V_{\text{sc}}(z, y)$ is a sort of scattering potential defined as

$$V_{\text{sc}}(z, y) = \begin{cases} -\omega^2(\epsilon_{\text{eff}} - \epsilon_0)\mu_0 + i\omega\mu_0\sigma_{\text{eff}} & \text{in catalyst,} \\ -\omega^2(\epsilon_{\text{q}} - \epsilon_0)\mu_0 + i\omega\mu_0\sigma_{\text{q}} & \text{in quartz,} \\ 0 & \text{in other reagion,} \end{cases} \tag{8}$$

where ϵ_{q} and σ_{q} are the dielectric constant and conductivity of the quartz tube. Although, in the ferroelectric metal such as nickel film, the energy loss is induced by the spin scattering or the eddy current, the permeability is assumed to be uniform and equal to μ_0. The effect induced by the variation of the permeability is now under consideration and will be discussed separately. The solution of eq. (7) must satisfy the boundary condition

$$\Phi(z, y) = \begin{cases} e^{ik_0 z} + \sum_p r_p e^{i(G_p y - k_p z)} & z < 0, \\ \sum_p t_p e^{i(G_p y + k_p z)} & z > L_{\text{W}}, \end{cases} \tag{9}$$

where $L_{\text{W}} = 2R_2$, $k_p = (\omega^2\epsilon_0\mu_0 - G_p^2)^{1/2}$, and $G_p = 2\pi p/L$ $(p = 0, \pm1, \pm2, \ldots)$ with L being the system size along the y-axis.

The partial differential equation (7) for the scattering wave can be reduced to an ordinary differential equation using a Fourier transformation along the y-axis. This ordinary differential equation can be transformed into a difference equation of the second order and its solution can be obtained numerically. This formulation to solve the scattering equation is developed in the area of solid-state physics.[8] We will apply this formulation to analyze the electromagnetic wave. When the wave $\Phi(x, y)$ is transformed to the Fourier series as $\Phi(z, y) = \sum_p \phi_p(z)\exp(iG_p y)$, the eq. (7) is reduced as follows,

$$\frac{d^2}{dz^2}\phi_p + \sum_q [v_{p-q} + (\omega^2\epsilon_0\mu_0 - G_p^2)\delta_{pq}]\phi_q = 0, \tag{10}$$

where $v_p(z)$ is the Fourier transformation of eq. (8) with respect to the y-axis. By introducing a vector $\Psi(z) = \{\phi_p(z)\}$ and a matrix $V(z) = [v_{p-q}(z) + (\omega^2\epsilon_0\mu_0 - G_p^2)\delta_{pq}]$, eq. (10) can be expressed as

$$\frac{d^2}{dz^2}\Psi + V\Psi = 0. \tag{11}$$

3.3 Scattering formulation by recursive transfer method

We use a discrete coordinate along the z-axis defined as $z = hn$ $(n = 0, 1, 2, \ldots, N)$ with an interval h and introducing a scattering matrix S_n defined as

$$\Psi(hn + h) = S_n\Psi(hn). \tag{12}$$

Then, eq. (11) is transformed into a difference equation such as

$$S_{n-1} = -(a_n S_n + b_n)^{-1}c_n, \tag{13}$$

where the matrices a_n, b_n, and c_n are defined as

$$a_n = I + \frac{h^2}{12}V(hn + h), \tag{14}$$

$$b_n = -2I + \frac{h^2}{6}V(hn), \tag{15}$$

$$c_n = I + \frac{h^2}{12}V(hn - h), \tag{16}$$

with the unit matrix I.

By using the matrix S_n and the vector $\Psi(hn)$, the boundary condition (9) is expressed as

$$S_n \to [e^{ik_p h}\delta_{pq}], \qquad (n \to N), \tag{17}$$

$$\Psi(hn) \to \Psi_{\text{in}} + \Psi_{\text{rf}}, \qquad (n \to 0), \tag{18}$$

with a wave number $k_p = (\omega^2\epsilon_0\mu_0 - G_p^2)^{1/2}$, an input vector $\Psi_{\text{in}} = \{\delta_{p0}\}$, and a reflection vector $\Psi_{\text{rf}} = \{r_p\}$, where r_p is the reflection coefficient introduced in the Fourier series of eq. (9).

By using the relation (13) and the condition (17), all matrices S_n are determined recursively from S_N $(= [\exp(ik_p h)\delta_{pq}])$. Consequently, the state vectors $\Psi(nh)$ are obtained successively from $\Psi(0)(= \Psi_{\text{in}} + \Psi_{\text{rf}})$ using the condition (18) and the relation (12). This is the origin of the name, recursive transfer method. The reflection vector Ψ_{rf} and the transmission vector $\Psi_{\text{tr}} = \{t_p\}$, where t_p is the transmission coefficient introduced in eq. (9), are expressed as follows,

$$\Psi_{\text{rf}} = -(S_0 - K_-)^{-1}(S_0 - K_+)\Psi_{\text{in}}, \tag{19}$$

$$\Psi_{\text{tr}} = K_-^N S_{N-1}\cdots S_2 S_1 S_0(\Psi_{\text{in}} + \Psi_{\text{rf}}), \tag{20}$$

where $K_+ = [\exp(ik_p h)\delta_{pq}]$ and $K_- = K_+^{-1}$.

3.4 Microwave absorption

The magnetic field can be derived from the formula $\mathbf{H} = \nabla \times \mathbf{E}/i\omega$, and the energy flux is expressed by the Poynting vector $\mathbf{E} \times \mathbf{H}$. When the Poynting vector is averaged over the y-axis and time domain, only the z-component remains. By using the reflection and transmission coefficients, r_p and t_p, which are the components of the vectors Ψ_{rf} and Ψ_{tr}, the nonzero flux components are determined as,

$$S_{\text{in}} = \frac{1}{2\eta}, \tag{21}$$

$$S_{\text{rf}} = \frac{1}{2\omega\mu_0}\sum_p |r_p|^2 k_p, \tag{22}$$

$$S_{\text{tr}} = \frac{1}{2\omega\mu_0}\sum_p |t_p|^2 k_p \tag{23}$$

for input, reflection and transmission waves, respectively. Here, η is defined as $\eta = (\mu_0/\epsilon_0)^{1/2}$. The reflection rate R and transmission rate T are defined as $R = S_{\text{rf}}/S_{\text{in}}$ and $T = S_{\text{tr}}/S_{\text{in}}$, respectively. The absorption by the catalyst, P_{abs}, is given as

$$P_{\text{abs}} = 1 - R - T. \tag{24}$$

3.5 *Comparison of theory and experiment*

Assuming that the temperature of the catalysis is proportional to the microwave absorption, the simulation data obtained by the recursive transfer method (solid curve) and the measurement data (circles and triangles) are compared in Fig. 5. The measurement data are for the catalyst calcined at 773 K (a) and 573 K (b). In Fig. 5(a), the maximum values of the simulation data and the measurement data are normalized as unity and aligned with each other. The relative value between (a) and (b) remains the same in the Fig. 2, since the data in Fig. 5(b) are normalized using the same factor used for Fig. 5(a).

The parameters used in the numerical calculation are listed in Table II, whose values are selected so as to fit the simulation and the experiment data. The resistance of (a) has been chosen to be smaller than that for (b), because the high calcination temperature causes to reduces the oxide. The increase in r_{neck} causes to suppress the maximum of the fitting curve in Fig. 5(b). The dimensions of the system and the model parameters are as follows. For the quartz tube, $R_1 = 7.5\,\text{mm}$, $R_2 = 9\,\text{mm}$, $\epsilon_q/\epsilon_0 = 3.8$, $\sigma_q = 0$. The parameters of the grain are $R_s = 100\,\mu\text{m}$, $\epsilon_s/\epsilon_0 = 3.8$, and $\sigma_s = 0$.

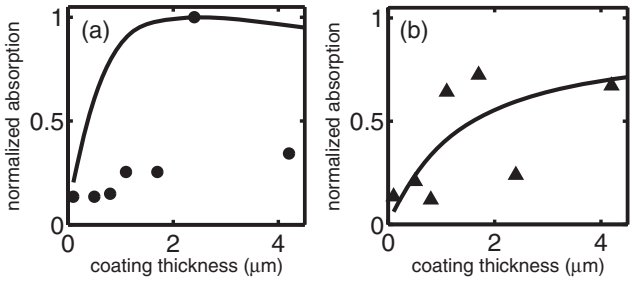

Fig. 5. Comparison of normalized absorption and measured data obtained from catalyst calcinated at 773 K (a) and 573 K (b).

Table II. Fitting parameters selected for the Fig. 5(a) and 5(b).

Fitting parameter	r_{neck} (kΩ)	ρ_{cr} ($10^{-3}\,\Omega\,\text{m}$)
(a)	0.11	9.37
(b)	7.50	31.2

In Fig. 6(a) and 6(b), the relationship between the coating thickness l and the parameters for the compound grains are shown, which are the effective skin depth δ_{eff}, effective dielectric constant ϵ_{eff}, effective conductance σ_{eff}, and filling factor f. The vertical axis for the effective conductance σ_{eff} is given in the right-hand side and normalized using the conductance of the pure nickel $\sigma_m = 4.44 \times 10^6\ (\Omega\,\text{m})^{-1}$. Each of (a) and (b) in Fig. 6 corresponds to (a) and (b) in Fig. 5, respectively.

Although, the variation of the filling factor, f, against the coating thickness l is relatively small, the effective dielectric constant ϵ_{eff} changes by about 10% and the effective conductance σ_{eff} changes more than two times in magnitude. The change in σ_{eff} involves the decrease in the effective skin depth δ_{eff}. Because the resistance parameters of (a) are smaller than those of (b) as shown in Table II, the effective skin depth δ_{eff} decreases rapidly in comparison with that in (b).

In Fig. 7, the field strength of the microwave is shown for various coating thicknesses l, where the solid circles indicate the outer fringe of the tube and the dashed circles represent the inner fringe. The fitting parameters are given in Table II(a). When the coating thickness l is less than 0.5 μm, the microwave can penetrate into the tube, as shown in Fig. 7(a). However, the absorption is small because the mass of the absorber (i.e., metal) is not much. On the other hand, when the coating film thickness l is larger than 5 μm, the microwave penetrates less into the tube, as shown in Fig. 7(c). Although the mass absorber (i.e., metal) is in the tube, the microwave is drained because the effective conductance σ_{eff} becomes large and the skin depth defined as $\delta_{\text{eff}} = (2/\omega\sigma_{\text{eff}}\mu_0)^{1/2}$ is much smaller than the radius of the quartz tube.

Although the theory can explain the experimental tendency, there remains a certain discrepancy between the measured and theoretical values. A possible reason is the

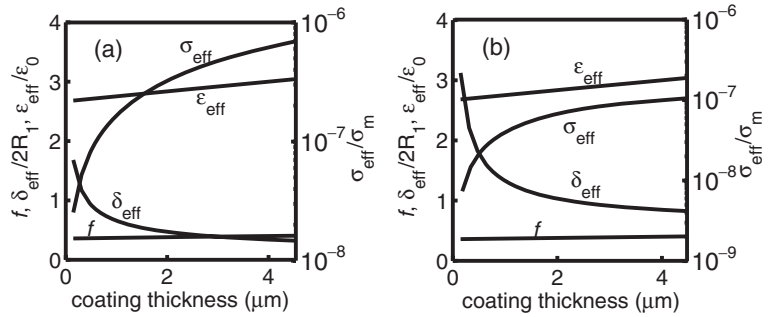

Fig. 6. Relationship between coating film thickness l and effective skin depth δ_{eff}, effective dielectric constant ϵ_{eff}, effective conductance σ_{eff}, and filling factor f. Each of (a) and (b) corresponds to the diagram of (a) and (b) in Fig. 5, respectively.

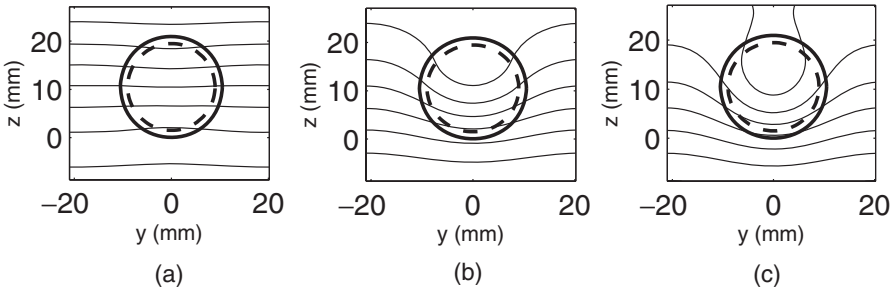

Fig. 7. Contour plot of field $\Phi(z, y)$ for various coating thicknesses l of metal on catalyst grain. The values of the fitting parameters are given in Table II(a). The film thicknesses l are 1 μm (a), 2 μm (b), and 5 μm (c), respectively.

distribution of the grain size and lack of uniformity of the neck resistance between the nesting grains. The distribution of grain size affects the value of the filling factor f. The oxide layer on the catalyst film causes unexpected fluctuations of the neck resistance r_{neck}. Unexpected lack of uniformity of microwave irradiation is also involved in the geometrical complexity of the system. An experiment concerning the simplified geometrical configuration is now underway and the results will be published in the near future.

4. Conclusions

In this paper, a phenomenological model to deal with a catalyst coated on quartz grain is proposed. The electric feature of the grains is characterized by the effective dielectric constant and the effective conductivity. The absorption is affected by the effective skin depth and the diameter of the container tube, and the peak in the absorption curve is explained by considering the crossover between the decrease in skin depth and the increase in catalyst mass associated with the catalyst thickness.

1) M. Park, S. Komarneni, and R. Roy: Mater. Lett. **43** (2000) 259.
2) K. Kamizaki, A. Yamamoto, K. Futami, K. Okayasu, and K. Yamauchi: Japan Patent Publication 08-99018 (1996).
3) S. Kato, K. Ito, H. Soga, and K. Tada: Japan Patent Publication 2000-334062 (2000).
4) M. Fang, J. Ma, P. Li, N. T. Lau, B. Zhu, and X. Lu: Appl. Catal. A **159** (1997) 211.
5) N. Lingaiah, P. S. S. Prasad, P. K. Rao, F. J. Berry, and L. E. Smart: Catal. Commun. **3** (2002) 391.
6) F. J. Berry, L. E. Smart, P. S. S. Prasad, N. Lingaiah, and P. K. Rao: Appl. Catal. A **204** (2000) 191.
7) R. Higuchi, H. Takashima, H. Kato, and Y. Kanno: Proc. IEEE Int. Conf. Systems, Man, and Cybernetics, Oct. 8–11, Taipei, Taiwan, 2006, p. 1408.
8) K. Hirose and M. Tsukada: Phys. Rev. B **51** (1995) 5278.
9) C. Kittel: *Introduction to Solid State Physics* (Wiley, New York, 2005) 8th ed., p. 464.